A new decoupling strategy for structures with frequency-dependent properties.

M. Geuzaine[a,b,c,d,*], J. Heremans[c,d], O. Øiseth[b], V. Denoël[c]

[a] NatHaz Modeling Laboratory, University of Notre Dame, USA
[b] Structural Engineering Department, NTNU Trondheim, Norway
[c] Structural & Stochastic Dynamics, University of LiÃšge, Belgium
[d] National Fund for Scientific Research, Brussels, Belgium

Abstract

In this paper, a new procedure is developed to decouple the governing equations of non-classically damped structures with frequency dependent properties. To start, a modal state formulation is used to eliminate the off-diagonal elements that damping might otherwise create in the transfer matrix. From there on, the transfer matrix is expanded in series and decoupling is achieved through an iterative scheme, which relies on the successive inversions of a diagonal matrix only. This approach is finally shown to converge fast and to perform well on the hydroelastic responses of a floating bridge.

Keywords: decoupling, frequency-dependent, power spectral density, variance, correlation

1. Nomenclature

Lowercase and capital bold letters are respectively used to denote vectors and matrices while italic letters with indices designate their elements. The superscripts $(.)^*$, $(.)^\intercal$ and $(.)^\dagger$ stand for the conjugate, the transpose and the hermitian operators. The imaginary unit is noted i and ω stands for the circular frequency.

2. Introduction

The dynamics of various civil engineering systems are governed by a set of second order differential equations whose Fourier transform reads

$$\mathbf{x}(\omega) = \left[\mathbf{K}(\omega) + i\omega\mathbf{C}(\omega) - \omega^2\mathbf{M}(\omega)\right]^{-1}\mathbf{f}(\omega) \tag{1}$$

where $\mathbf{K}(\omega)$, $\mathbf{C}(\omega)$ and $\mathbf{M}(\omega)$ represent frequency-dependent stiffness, damping, and mass matrices. Meanwhile, the two vectors $\mathbf{f}(\omega)$ and $\mathbf{x}(\omega)$ respectively correspond to the frequency-domain representation of the external loads and the structural motions.

Among other fields of application [1], Equation (1) is suitable to describe energy dissipation and fluid-structure interaction in linear settings (e.g. for the aeroelastic and hydroelastic analysis of bridges). In such circumstances, the stiffness, damping, and mass matrices are usually composed of static and added parts as follows: $\mathbf{K}(\omega) = \mathbf{K}_\mathrm{s} + \mathbf{K}_\mathrm{a}(\omega)$, $\mathbf{C}(\omega) = \mathbf{C}_\mathrm{s} + \mathbf{C}_\mathrm{a}(\omega)$, and $\mathbf{M}(\omega) = \mathbf{M}_\mathrm{s} + \mathbf{M}_\mathrm{a}(\omega)$. This formulation is generic though. Some components may also drop according to the situation (*e.g.* in [2, 3]).

*corresponding author, preprint submitted to Mechanical Systems and Signal Processing, May 10, 2023

Yet, in common practice, the external loads and the structural motions are assumed to be gaussian and stationary. Their mean values are also treated apart thanks to the linear nature of Equation (1). As a result, their probabilistic properties are fully described by their respective power spectral densities (PSDs), $\mathbf{S}_{\mathrm{f}}(\omega)$ and $\mathbf{S}_{\mathrm{x}}(\omega)$. For instance, the diagonal elements of

$$\boldsymbol{\Sigma}_{\mathrm{x}} = \int_{-\infty}^{+\infty} \mathbf{S}_{\mathrm{x}}(\omega)\,\mathrm{d}\omega \quad \text{and} \quad \boldsymbol{\Sigma}_{\dot{\mathrm{x}}} = \int_{-\infty}^{+\infty} \omega^2 \mathbf{S}_{\mathrm{x}}(\omega)\,\mathrm{d}\omega \quad \text{with} \quad \mathbf{S}_{\mathrm{x}}(\omega) = \mathbf{x}(\omega)\,\mathbf{x}^*(\omega) \tag{2}$$

correspond to the variances of both the structural responses and their time derivatives.

These statistics, in particular, are essential for design perspectives. Unfortunately, civil engineering structures can be composed of N degrees-of-freedom with N reaching up to several thousands. In consequence, inverting $\left[\mathbf{K}(\omega) + i\omega\mathbf{C}(\omega) - \omega^2\mathbf{M}(\omega)\right]$ of size $N \times N$ to calculate the transfer matrix at all circular frequencies can be extremely demanding. To reduce this computational burden, the structural responses are commonly projected into a subspace formed by a limited number $M \ll N$ of modes.

This approach generally intends to decouple the governing equations as well, so that they can be solved individually without having to invert full matrices anymore. Such an interesting advantage is however subject to the condition that the stiffness, damping, and mass matrices are simultaneously diagonalizable. But this cannot be ensured when (i) the added damping is not necessarily proportional to the added mass and stiffness matrices [4], and (ii) these three matrices are supposed to vary with the frequency [5].

Despite these difficulties, two methods claim to be able to decouple the governing equations, if not exactly at least appproximately. First, in [2], a quasi-diagonal state-space formulation is developed for the transfer matrix of linear mechanical systems with frequency-dependent viscoelastic properties. The mass matrix still needs to be inverted, but only once because it is independent of the frequency. Otherwise, though, this approach is not adequate and this is the reason why it cannot be applied in the present context.

Second, in [6], the approximate formulation of the transfer matrix developed by [7] is used to perform the analysis of a two degree-of-freedom system subjected to aeroelastic loads in the physical space. This approach is valid no matter the mass matrix, as long as the transfer matrix is diagonally dominant [8]. The issue there is that it is shown to work for small damping levels of about 0.5%, but not for moderate damping levels of up to 5.0% which reduces the diagonal dominance of the transfer matrix.

In the present paper, a new method is proposed to solve this last problem. By contrast with [6], the governing equations are expressed in state-space first and are then projected into a complex modal basis. The coupling induced by the non-classicity of the damping is therefore eliminated before making use of the approximate formulation suggested in [7] for the transfer matrix. Hence, its diagonal dominance and the series convergence are improved.

The capacity of this new procedure to decouple the equations of motions while providing accurate results for the statistics of the structural displacements and velocities is eventually demonstrated on the hydroelastic analysis of a floating bridge whose damping and mass matrices are frequency-dependent. In addition to featuring damping ratios of up to 10%, this structure also contains much more degrees-of-freedom than the aeroelastic pitch-plunge model studied in [6].

3. Proposed Methodology

3.1. State Space Eigenproblem

First, the state variables $\mathbf{y}(\omega) = \begin{bmatrix} \mathbf{I} & i\omega\mathbf{I} \end{bmatrix}^T \mathbf{x}(\omega)$ and the state forces $\mathbf{g}(\omega) = \begin{bmatrix} \mathbf{I} & \mathbf{0} \end{bmatrix}^T \mathbf{f}(\omega)$, with $\mathbf{I}$ and $\mathbf{0}$ being respectively the $N \times N$ identity and zero matrices, are introduced. Doing so allows to recast the initial set of N second-order equations into $2N$ first-order equations. Indeed, it yields

$$\mathbf{y}(\omega) = [\mathbf{A}(\omega) + i\omega\mathbf{B}(\omega)]^{-1}\,\mathbf{g}(\omega) \tag{3}$$

where

$$\mathbf{A}(\omega) = \begin{bmatrix} \mathbf{K}(\omega) & \mathbf{0} \\ \mathbf{0} & -\mathbf{M}(\omega) \end{bmatrix} \quad \text{and} \quad \mathbf{B}(\omega) = \begin{bmatrix} \mathbf{C}(\omega) & \mathbf{M}(\omega) \\ \mathbf{M}(\omega) & \mathbf{0} \end{bmatrix} \tag{4}$$

are referred to as the state matrices. These definitions of the state properties are chosen among others to conserve the symmetry of the stiffness, mass and damping matrices when applicable [9].

From there on, the left and right eigenproblems associated to the homogeneous part of the governing equations are written in the standard form

$$\boldsymbol{\theta}_{L,m}^T\,[\mathbf{A}(\Re[\Omega_m]) + i\Omega_m\mathbf{B}(\Re[\Omega_m])] = \mathbf{0} \quad \text{and} \quad [\mathbf{A}(\Re[\Omega_m]) + i\Omega_m\mathbf{B}(\Re[\Omega_m])]\,\boldsymbol{\theta}_{R,m} = \mathbf{0} \tag{5}$$

despite being nonlinear. They are subsequently solved with an iterative algorithm to get the eigenvalues, $\boldsymbol{\Omega} = \mathrm{diag}(\Omega_1, ..., \Omega_m, ..., \Omega_{2M})$, as well as the left and right eigenmodes, $\boldsymbol{\Theta}_L = [\boldsymbol{\theta}_{L,1}, ..., \boldsymbol{\theta}_{L,m}, ..., \boldsymbol{\theta}_{L,2M}]$ and $\boldsymbol{\Theta}_R = [\boldsymbol{\theta}_{R,1}, ..., \boldsymbol{\theta}_{R,m}, ..., \boldsymbol{\theta}_{R,2M}]$. These complex eigensolutions are then sorted to ensure that

$$\Omega_m = \Psi_m + i\,\Upsilon_m \quad \text{with} \quad \Psi_m = (-1)^m\sqrt{1-\xi_{j_m}^2}\,\omega_{j_m} \quad \text{and} \quad \Upsilon_m = \xi_{j_m}\,\omega_{j_m} \tag{6}$$

where ω_{j_m} and ξ_{j_m} correspond to the $j_m = \left\lceil \frac{m}{2} \right\rceil$-th natural frequency and damping ratio of the structure.

The eigenmodes of odd (resp. even) rank are also normalized by the maximum absolute value of their real (resp. imaginary) part. They are used afterwards to create a subspace in which the first $2M \ll 2N$ modal state responses are known to provide an accurate description of the structural dynamics. With such a formulation, the coupling caused by the non-classical nature of the damping is eliminated.

Indeed, being just two instead of three, the state matrices are simultaneously diagonalizable by $\boldsymbol{\Theta}_L$ and $\boldsymbol{\Theta}_R$ no matter the damping, provided that the properties of the structure are not frequency-dependent. But otherwise, the eigenvectors are not orthogonal through $\mathbf{A}(\omega)$ and $\mathbf{B}(\omega)$. Hence, the dynamical flexibility matrix

$$\boldsymbol{\mathcal{J}}(\omega) = \boldsymbol{\mathcal{A}}(\omega) + i\omega\boldsymbol{\mathcal{B}}(\omega) \quad \text{where} \quad \boldsymbol{\mathcal{A}}(\omega) = \boldsymbol{\Theta}_L^T\mathbf{A}(\omega)\,\boldsymbol{\Theta}_R \quad \text{and} \quad \boldsymbol{\mathcal{B}}(\omega) = \boldsymbol{\Theta}_L^T\mathbf{B}(\omega)\,\boldsymbol{\Theta}_R \tag{7}$$

contains non-zero off-diagonal elements unless the stiffness, damping and mass matrices are constant.

3.2. Modal State Responses

In consequence, substituting the modal projection $\mathbf{p}(\omega) = \boldsymbol{\Theta}_L^T\mathbf{g}(\omega)$ and the modal decomposition $\mathbf{y}(\omega) = \boldsymbol{\Theta}_R\mathbf{q}(\omega)$ into Equation (3) yields

$$\mathbf{q}(\omega) = [\boldsymbol{\mathcal{J}}(\omega)]^{-1}\mathbf{p}(\omega) \tag{8}$$

for the modal state responses but does not decouple the system. To consider each mode separately, it is proposed to introduce the alternative expression

$$[\boldsymbol{\mathcal{J}}(\omega)]^{-1} = \left[\mathbf{I} + \sum_{k=1}^{+\infty} (-1)^k \left(\boldsymbol{\mathcal{J}}_{\mathrm{d}}^{-1}(\omega)\,\boldsymbol{\mathcal{J}}_{\mathrm{o}}(\omega)\right)^k\right] \boldsymbol{\mathcal{J}}_{\mathrm{d}}^{-1}(\omega) \tag{9}$$

where $\boldsymbol{\mathcal{J}}_{\mathrm{d}}(\omega)$ and $\boldsymbol{\mathcal{J}}_{\mathrm{o}}(\omega)$ respectively collect the diagonal and the off-diagonal elements of $\boldsymbol{\mathcal{J}}(\omega)$ [7]. The inversion of a full matrix is no longer required with this formula. However, because of matrix multiplications, using it can only reduce the computational demand if the series can be truncated at a sufficiently low order.

Fortunately enough, this series is proven to converge provided that the diagonality index of $\boldsymbol{\mathcal{J}}(\omega)$ is less than unity [7, 6]. This parameter is defined by

$$\delta(\boldsymbol{\mathcal{J}}(\omega)) = \max\left[\mathrm{eig}\left(\boldsymbol{\mathcal{J}}_{\mathrm{d}}^{-1}(\omega)\,\boldsymbol{\mathcal{J}}_{\mathrm{o}}(\omega)\right)\right] \tag{10}$$

and measures the importance of the coupling terms in the dynamical flexibility matrix. If the elements of $\boldsymbol{\mathcal{J}}_o(\omega)$ are extremely small, so is the diagonality index. In this event, $\boldsymbol{\mathcal{J}}(\omega)$ can be replaced by $\boldsymbol{\mathcal{J}}_{\mathrm{d}}(\omega)$ in Equation (8) and the modal state responses can be given by

$$\mathbf{q}_{\mathrm{d}}(\omega) = \boldsymbol{\mathcal{H}}_{\mathrm{d}}(\omega)\,\mathbf{p}(\omega) \tag{11}$$

where $\boldsymbol{\mathcal{H}}_{\mathrm{d}}(\omega) = \boldsymbol{\mathcal{J}}_{\mathrm{d}}^{-1}(\omega)$ collects frequency response functions on its diagonal and zeros everywhere else. This matrix is therefore diagonal, which means that the modal state responses are decoupled and can be determined independently of one another.

If it is not enough to reach the desired level of accuracy, an iterative procedure can be initiated. Starting with $\Delta\mathbf{q}_0(\omega) = \mathbf{q}_{\mathrm{d}}(\omega)$, a new set of modal state forces can be computed by $\Delta\mathbf{p}_1(\omega) = -\boldsymbol{\mathcal{J}}_{\mathrm{o}}(\omega)\,\Delta\mathbf{q}_0(\omega)$. It can then be applied to the same decoupled system as before to give the corrections of the modal state responses as follows $\Delta\mathbf{q}_1(\omega) = \boldsymbol{\mathcal{H}}_{\mathrm{d}}(\omega)\,\Delta\mathbf{p}_1(\omega)$. These terms can finally be used to define a new set of modal state forces, and so on (see Figure 1). In the sequel, though, the modal coupling is assumed to be correctly taken into account when stopping the procedure at first order and the modal state responses therefore read $\mathbf{q}_1(\omega) = \Delta\mathbf{q}_0(\omega) + \Delta\mathbf{q}_1(\omega)$.

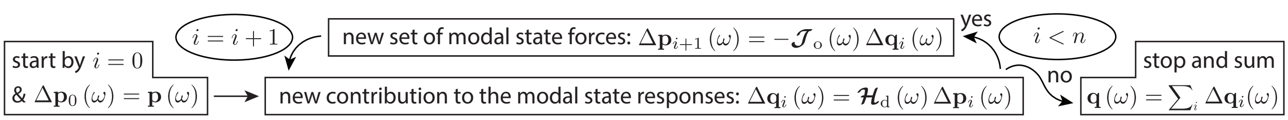

Figure 1: Flowchart of the iterative procedure presented hereabove, with n being the truncation order.

3.3. Power Spectral Densities

The power spectral densities of the forces are initially expressed in the physical coordinates and gathered in the matrix $\mathbf{S}_{\mathrm{f}}(\omega)$. They can subsequently enter in the determination of the matrix

$$\mathbf{S}_{\mathrm{g}}(\omega) = \begin{bmatrix} \mathbf{S}_{\mathrm{f}}(\omega) & \mathbf{0} \\ \mathbf{0} & \mathbf{0} \end{bmatrix} \tag{12}$$

which contains the power spectral densities of the state forces. It then yields the power spectral densities of the modal state forces. They are given by

$$\mathbf{S}_{\mathrm{p}}(\omega) = \boldsymbol{\Theta}_L^T \mathbf{S}_{\mathrm{g}}(\omega)\, \boldsymbol{\Theta}_L^* \tag{13}$$

after projection. The power spectral densities of the modal state responses are finally computed as follows

$$\mathbf{S}_{\mathrm{q}}(\omega) = \boldsymbol{\mathcal{H}}(\omega)\, \mathbf{S}_{\mathrm{p}}(\omega)\, \boldsymbol{\mathcal{H}}^\dagger(\omega) \tag{14}$$

where $\boldsymbol{\mathcal{H}}(\omega) = [\boldsymbol{\mathcal{J}}(\omega)]^{-1}$ represents the transfer matrix of the system.

Introducing the series expansion of the dynamical flexibility matrix into Equation (14) and truncating it at first order allows to estimate the power spectral densities of the modal state responses as the sum of a leading order term and a first order term which respectively read

$$\mathbf{S}_{\mathrm{q}_0}(\omega) = \boldsymbol{\mathcal{H}}_{\mathrm{d}}(\omega)\, \mathbf{S}_{\mathrm{p}}(\omega)\, \boldsymbol{\mathcal{H}}_{\mathrm{d}}^\dagger(\omega) \tag{15}$$

and

$$\mathbf{S}_{\mathrm{q}_{0/1}}(\omega) = -\boldsymbol{\mathcal{H}}_{\mathrm{d}}(\omega)\, \boldsymbol{\mathcal{J}}_{\mathrm{o}}(\omega)\, \mathbf{S}_{\mathrm{q}_0}(\omega) - \mathbf{S}_{\mathrm{q}_0}^\dagger(\omega)\, \boldsymbol{\mathcal{J}}_{\mathrm{o}}^\dagger(\omega)\, \boldsymbol{\mathcal{H}}_{\mathrm{d}}^\dagger(\omega) \tag{16}$$

whereas the next correction is directly discarded on the basis that it is a second order term [10]. The approximations of the power spectral densities are eventually given by

$$\mathbf{S}_{\mathrm{q}_1}(\omega) = \mathbf{S}_{\mathrm{q}_0}(\omega) + \mathbf{S}_{\mathrm{q}_{0/1}}(\omega) \tag{17}$$

and do not require to invert a full matrix again anymore.

As indicated in [10], the corrections provided at first order are necessary to approximate the off-diagonal elements $\mathbf{S}_{\mathrm{q}}(\omega)$ even though they are globally small with respect to the leading terms in $\mathbf{S}_{\mathrm{q}_0}(\omega)$. When the modal state forces are uncorrelated indeed, $\mathbf{S}_{\mathrm{q}_0}(\omega)$ is transformed into a diagonal matrix. As a consequence, the off-diagonal elements of $\mathbf{S}_{\mathrm{q}_1}(\omega)$ are exclusively given by $\mathbf{S}_{\mathrm{q}_{0/1}}(\omega)$ in this specific case. The corrective terms are hence to be compared with zeros and are therefore not negligible, no matter their smallness. On the other hand, they completely disappear if the dynamical flexibility matrix is diagonal, or considered as such.

3.4. Second Order Statistics

At last, the power spectral densities of the modal state responses obtained in the previous section can be integrated to provide the second order statistics of the corresponding processes. These scalar values can then be recombined to get the same results for the nodal state responses. This process reads

$$\boldsymbol{\Sigma}_{\mathrm{y}_\star} = \boldsymbol{\Theta}_R \boldsymbol{\Sigma}_{\mathrm{q}_\star} \boldsymbol{\Theta}_R^\dagger \quad \text{with} \quad \boldsymbol{\Sigma}_{\mathrm{q}_\star} = \int_{-\infty}^{+\infty} \mathbf{S}_{\mathrm{q}_\star}(\omega)\, \mathrm{d}\omega \tag{18}$$

where the star subscript denotes nothing, 0, 0/1 or 1 depending on whether the PSDs from Eq. (14), Eq. (15), Eq. (16) or Eq. (17) are selected.

In order to provide a fair evaluation of the importance that the modal covariances might have as compared to the modal variances, Equation (18) can also be rewritten as follows

$$\Sigma_{y_\star,ij} \quad = \quad \Theta_{R,im}\Theta_{R,jm}^* \Sigma_{q_\star,mm} + \sum_{m=1}^{2N} \sum_{n=1,n\neq m}^{2N} \Theta_{R,im}\Theta_{R,jn}^* \rho_{q_\star,mn} \sqrt{\Sigma_{q_\star,mm}\Sigma_{q_\star,nn}} \tag{19}$$

where

$$\rho_{q_\star,mn} = \frac{\Sigma_{q_\star,mn}}{\sqrt{\Sigma_{q_\star,mm}\Sigma_{q_\star,nn}}} \tag{20}$$

are the correlation coefficients of the m-th and n-th modal state responses. These coefficients are indeed easier to compare because they are dimensionless and bounded in the interval $[-1, 1]$.

Through the definition of the state variables, the second order statistics of the nodal responses in the state coordinates also end up reading

$$\mathbf{\Sigma}_{\mathrm{y}} = \mathbb{E}\begin{bmatrix} \mathbf{x}(\omega)\,\mathbf{x}^*(\omega) & \mathbf{x}(\omega)\,\dot{\mathbf{x}}^*(\omega) \\ \dot{\mathbf{x}}(\omega)\,\mathbf{x}^*(\omega) & \dot{\mathbf{x}}(\omega)\,\dot{\mathbf{x}}^*(\omega) \end{bmatrix} \tag{21}$$

since $\dot{\mathbf{x}}(\omega) = i\omega\mathbf{x}(\omega)$. It indicates that the top left and the bottom right blocks of size $N \times N$ in Equation (18) correspond to the second order statistics of either the structural motions, either the structural velocities shown in Equation (2).

4. Case Study: Hydroelastic Analysis of a Floating Bridge

4.1. Models

The methodology proposed in this paper is now used to perform the hydroelastic analysis of an end-anchored floating pontoon bridge subjected to first order wave loads [3]. This example is based on a two-dimensional finite element model of the BergsÃžysund Bridge, which crosses a 300-m deep fjord in the Northwestern coast of Norway and is currently the longest of its kind.

As illustrated in Figure 2-(a) and Figure 2-(b), this bridge is composed of seven pontoons which are connected to each others and to the banks by 105-m and 151.5-m long beam sections, respectively. The locations and orientations of the pontoons are listed in Table 1. They are expressed in the coordinate system (x_1, x_2, x_3) which is introduced in Figure 2-(b).

Each bridge deck section is constituted of 20 equivalent beam elements whose characteristics are listed in Table 2. They are combined in a finite element framework to compute the static stiffness and mass matrices of the structure. Meanwhile, the static damping matrix is evaluated by $\mathbf{C}_s = \alpha_m \mathbf{M}_s + \alpha_k \mathbf{K}_s$ with $\alpha_m = 9 \times 10^{-4}$ Hz and $\alpha_k = 11.02 \times 10^{-4}$ s.

Both the hydroelastic properties of the pontoons and the power spectral densities of the forces are then obtained as described in [3]. For the sake of conciseness, this paper can be consulted for details about their effective computation. Meanwhile, the main hypotheses, functions, and parameters involved in their determination are summarized hereafter.

As explained before, interactions between the motions of the fluid and the structure are accounted for by means of added stiffness, damping and mass matrices. In the present context, however, only the last two of them are effectively frequency-dependent. This is exemplified in Figure 2-(c) for one degree-of-freedom, which is actually representative of all others.

As regards to undisturbed waves, a two-parameter elevation spectrum and a cos-2s directional distribution are chosen [11, 3]. The values adopted for their input parameters (the significant wave height, the peak wave frequency and the spreading wave coefficient) are provided in Table 2. The preferred orientation of the waves is also set to be parallel to the x_2-axis.

Last but not least, the wave elevation-to-force operators are required. Just like the added damping and mass, these characteristics are established for each pontoon, considering that their surrounding wave field is not affected by the motion of the other pontoons. To do so, the potential flow solver implemented in the HydroD WADAM module is used as in [3].

4.2. Results

First, the nonlinear eigenvalue problems specified in Eq. (5) are solved in an iterative way to calculate the natural frequencies, damping ratios and mode shapes of the structure. These results are reported in Figure 3 for the first ten eigensolutions while the remaining ones are discarded for truncation purposes.

Second, the power spectral densities of the modal state responses are computed according to Eq. (14), Eq. (15), and Eq. (17). The reference functions, 0^{th} and 1^{st} order approximations thereby issued, as well as relative errors, are depicted by solid, dashed and dotted lines in Figure 4 for the 1^{st} and the 4^{th} modes.

Third, the statistics of the modal state responses are obtained after integration of the power spectral densities. Regarding the modal state variances, the reference and approximate outcomes at 0^{th} and 1^{st} order are compared in Figure 5-(a). Relative errors are also represented for each mode in Figure 5-(b).

Fourth, Eq. (20) is used to calculate the correlation coefficients. The reference values are illustrated in Figure 5-(c) and the first order approximate results are displayed in Figure 5-(d). The respective contributions of $\mathbf{\Sigma}_{\mathrm{q}_0}$ and $\mathbf{\Sigma}_{\mathrm{q}_{0/1}}$ are given as well in Figure 5-(e) and Figure 5-(f).

Fifth, the variances of the nodal state responses are reconstructed based on Eq. (18). The magnitudes of the displacements and the velocities are then evaluated as follows

$$m_x = \sqrt{\sigma_{x_1}^2 + \sigma_{x_2}^2} \quad ; \quad m_{\dot{x}} = \sqrt{\sigma_{\dot{x}_1}^2 + \sigma_{\dot{x}_2}^2}$$

for each formulation. They are represented in Figure 6-(a) and Figure 6-(b) while relative errors are shown in Figure 6-(a') and Figure 6-(b').

4.3. Analysis

A close agreement is observed between the reference and the approximate power spectral densities of the modal state responses in Figure 4-(a) and Figure 4-(b). In addition, the relative errors decrease when using the 1^{st} instead of 0^{th} order approximation. This phenomenon is however less pronounced for the first mode, in Figure 4-(a'), than for the fourth mode, in Figure 4-(b').

Owing to the compensation of positive and negative errors during the integration, though, this gain of accuracy disappears for the variance of the first modal state response. But apart from this minor detail, a genuine fit is observed again between the three solutions, see Figure 5-(a), and a rapid convergence is highlighted for all modes, see Figure 5-(b).

These trends are actually to be expected given that the series converges faster if the diagonality index of the dynamical flexibility matrix is smaller. Yet, as indicated in Figure 3, it reaches its peak value of 0.46 at

$\omega = 0.74$ rad/s, which is almost equal to the first natural frequency, and then drops to half this value at most over the rest of the frequency range.

Interestingly enough, the errors also appear to be less severe for the modes that are excited the most in their resonant regimes and influence therefore the most the response. This effect occurs more specifically for the third and the fourth modes, whose natural frequencies are very close to the peak frequency of the waves. Their resonant peaks thus appear where the PSDs of the forces are approaching their highest points, see Figure 4-(b) for instance.

Meanwhile, the first and the second modes respond almost exclusively in the inertial regime because the PSDs of the forces are exponentially small at low frequencies for linear waves and resonant amplifications are therefore annihilated below a given threshold. These differences can clearly be seen in Figure 4-(a) and Figure 4-(b). The smallness of the power spectral densities at low frequencies is also the reason why relative errors are not reliable, and therefore not shown in the grey bands of Figure 4-(a') and Figure 4-(b').

Then, in Figure 5-(c), two sets of modal state responses are identified as being correlated: the 1$^{\text{st}}$, the 4$^{\text{th}}$, the 6$^{\text{th}}$, the 8$^{\text{th}}$ and the 9$^{\text{th}}$ ones versus the 5$^{\text{th}}$, the 7$^{\text{th}}$ and the 10$^{\text{th}}$ ones. This is probably due to the symmetry proeprties of the associated modes and forces. The non-zero off-diagonal elements of $\mathbf{\Sigma}_{\mathrm{q}_0}$ in Figure 5-(e) also indicate that the modal state forces are correlated as well.

An excellent correspondence is achieved between the correlation coefficients too and this is demonstrated once more for the magnitudes of the displacement and velocities. In Figure 6-(a'), in particular, it appears that the relative errors are below 5.0% along the entire bridge with the approximation at 0$^{\text{th}}$ order and below 0.5% with the appproximation at first order.

5. Conclusions

The present paper proposes to combine a modal state formulation with a series expansion of the frequency response matrix to decouple the governing equations of a structure with frequency-dependent properties. This procedure indeed allows to compute the power spectral densities and the second order statistics of both the displacements and the velocities based on the successive inversions of a diagonal matrix only.

This approach is also iterative. It can be stopped at any order according to the desired level of precision, but it should be remembered that the higher the order, the higher the computational cost. It is consequently useful to notice that this process converges quickly and in an asymptotic sense as long as the diagonality index of the dynamical flexibility matrix is smaller than unity over the whole range of frequencies.

When using this methodology to conduct the hydroelastic analysis of a two-dimensional floating bridge, the approximations at first order gave values for the variances of the nodal responses with less than one percent error although the diagonality index was moderate, reaching a maximum value of about one half at some point. These outstanding results hence demonstrate that this method applies to realistic structures.

Overall, it is the first time that such a neat decoupling of the governing equations is achieved for a more than two degrees-of-freedom structure with frequency-dependent properties, which are characterized by non-classical damping ratios of more than 5%.

6. Acknowledgements

The first and the second authors received financial support from the F.R.S.-FNRS (Belgian Fund for Scientific Research). The work of the first author at NTNU Trondheim was also funded by two research stay grants of the FWB (FÃ©dÃ©ration Wallonie-Bruxelles) and the Rotary. The contribution of the Norwegian Public Road Administration is acknowledged as well by the third author.

References

[1] P. D. Spanos, B. A. Zeldin, Random Vibration of Systems with Frequency-Dependent Parameters or Fractional Derivatives, Journal of Engineering Mechanics 123 (3) (1997) 290–292. doi:10.1061/(asce)0733-9399(1997)123:3(290).

[2] F. Mastroddi, P. Calore, On the modal decoupling of linear mechanical systems with frequency-dependent viscoelastic behavior, Mechanical Systems and Signal Processing 70-71 (2016) 769–787. doi:10.1016/j.ymssp.2015.09.024.

[3] K. A. Kvåle, R. Sigbjörnsson, O. Øiseth, Modelling the stochastic dynamic behaviour of a pontoon bridge: A case study, Computers and Structures 165 (2016) 123–135. doi:10.1016/j.compstruc.2015.12.009.

[4] S. Adhikari, Optimal complex modes and an index of damping non-proportionality, Mechanical Systems and Signal Processing 18 (1) (2004) 1–27. doi:10.1016/S0888-3270(03)00048-7.

[5] L. Rouleau, J.-F. Deü, A. Legay, A comparison of model reduction techniques based on modal projection for structures with frequency-dependent damping, Mechanical Systems and Signal Processing 90 (2017) 110–125.

[6] J. Heremans, M. Geuzaine, V. Denoël, A Background/Resonant decomposition based method to predict the aeroelastic behavior of 2-dof aeroelastic oscillators, Journal of Wind Engineering and Industrial Aerodynamics 233 (2023) 105290.

[7] V. Denoël, H. Degée, Asymptotic expansion of slightly coupled modal dynamic transfer functions, Journal of Sound and Vibration 328 (1-2) (2009) 1–8. doi:10.1016/j.jsv.2009.08.014.

[8] M. Morzfeld, N. Ajavakom, F. Ma, Diagonal dominance of damping and the decoupling approximation in linear vibratory systems, Journal of Sound and Vibration 320 (1-2) (2009) 406–420. doi:10.1016/j.jsv.2008.07.025.

[9] A. Berthet, E. Perrey-Debain, J. D. Chazot, S. Germès, The balanced proper orthogonal decomposition applied to a class of frequency-dependent damped structures, Mechanical Systems and Signal Processing 185 (September 2022) (2023). doi:10.1016/j.ymssp.2022.109746.

[10] T. Canor, N. Blaise, V. Denoël, Efficient uncoupled stochastic analysis with non-proportional damping, Journal of Sound and Vibration 331 (24) (2012) 5283–5291. doi:10.1016/j.jsv.2012.07.019.

[11] M. Geuzaine, A. Fenerci, O. Øiseth, V. Denoël, Multiple Timescale Spectral Analysis of Floating Structures Subjected to Hydrodynamic Loads, Journal of Engineering Mechanics 149 (2023). doi:10.1061/JENMDT.EMENG-6654.

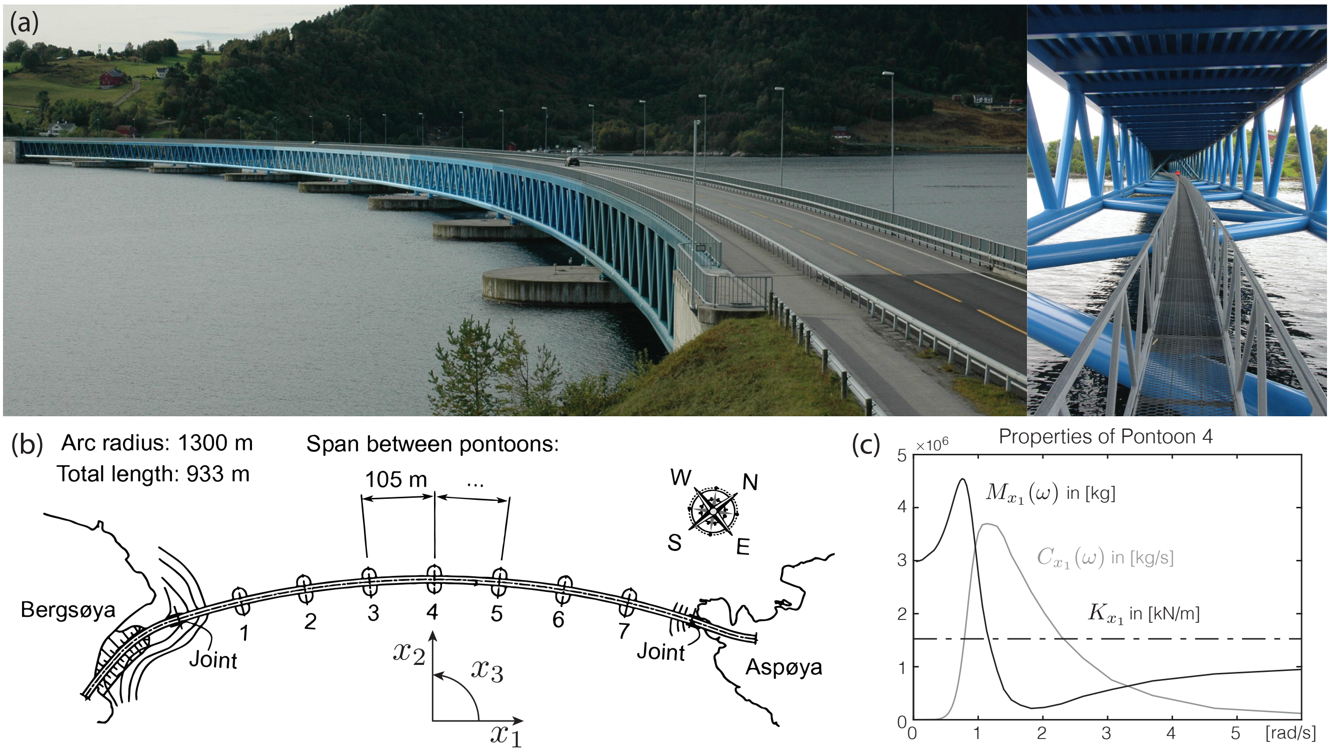

Figure 2: BergsÃžysund Bridge – (a) pictures, (b) details, as well as (c) the evolution of the added mass and the added damping associated to the x_1-displacement of Pontoon 4 with respect to the circular frequency.

Pontoon		1	2	3	4	5	6	7
X_1	[m]	-342	-230	-115	0	115	230	342
X_2	[m]	1254	1280	1295	1300	1295	1280	1254
X_3	[Â°]	104	99	95	90	85	81	76

Table 1: Locations and orientations of the pontoons.

Name	Value	Unit
Spreading Wave Constant	3	–
Significant Wave Height	2.4	m
Peak Wave Frequency	2.2	rad/s
Element Length	5.25	m
Inertia Moment	12.36	m^4
Young Modulus	2×10^{10}	N/m^2
Steel Density	7850	kg/m^3

Table 2: Parameters of the case study.

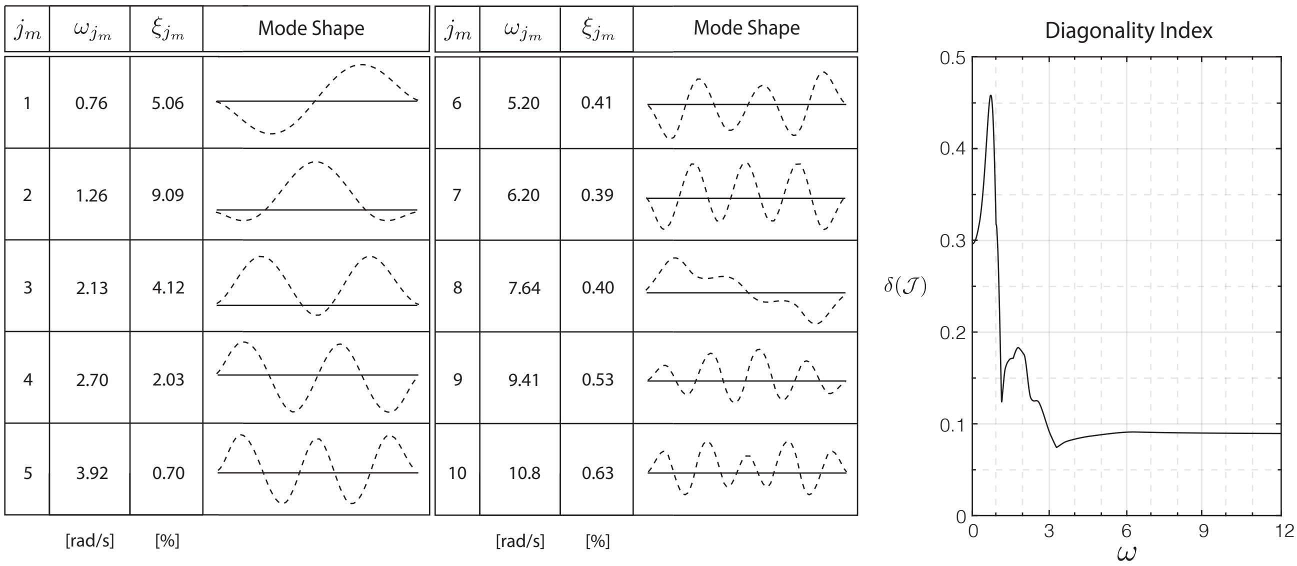

Figure 3: Results obtained for the modal analysis and the diagonality index of the considered bridge model.

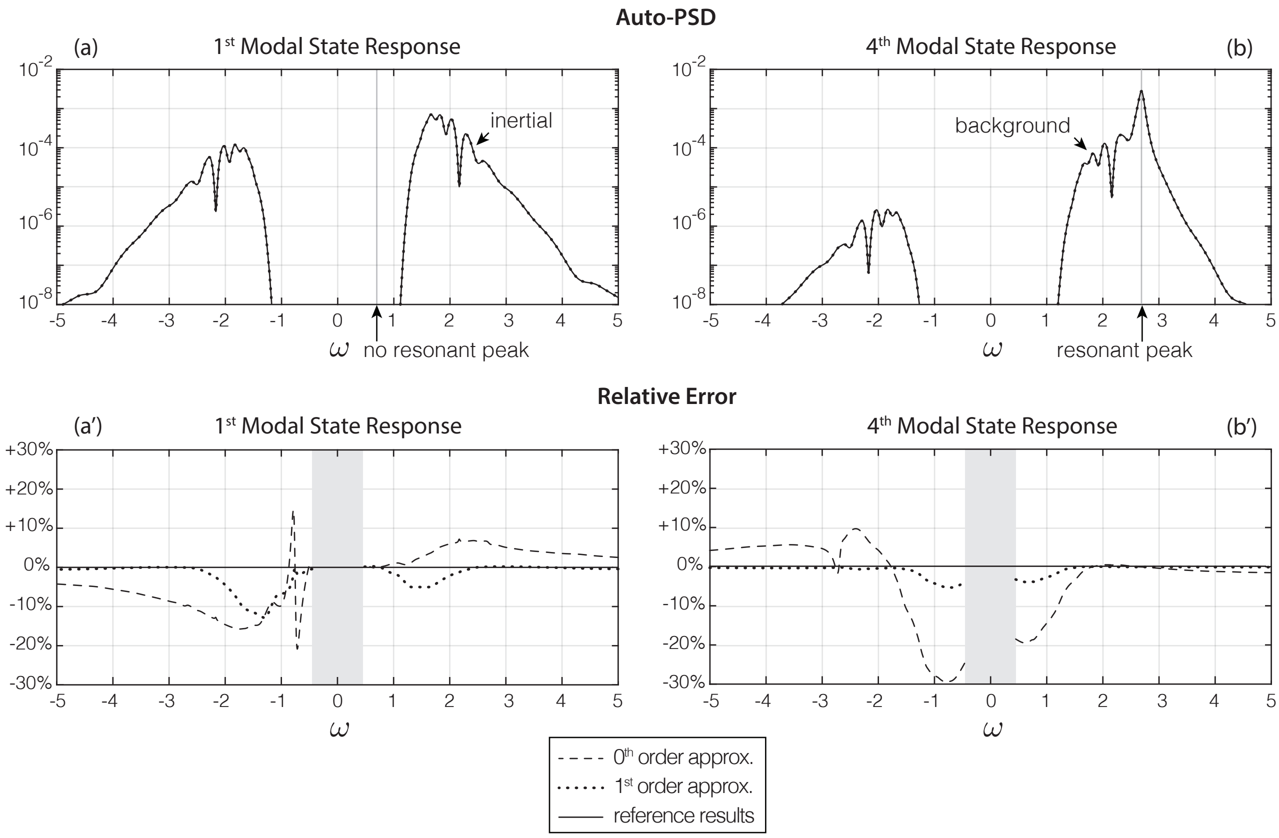

Figure 4: Reference and approximate auto-power spectral densities, as well as relative errors associated with each formulation, of (a)-(a') the first and (b)-(b') the fourth modal state responses. Please notice that the lack of symmetry in these functions is due to the use of a complex modal basis [11].

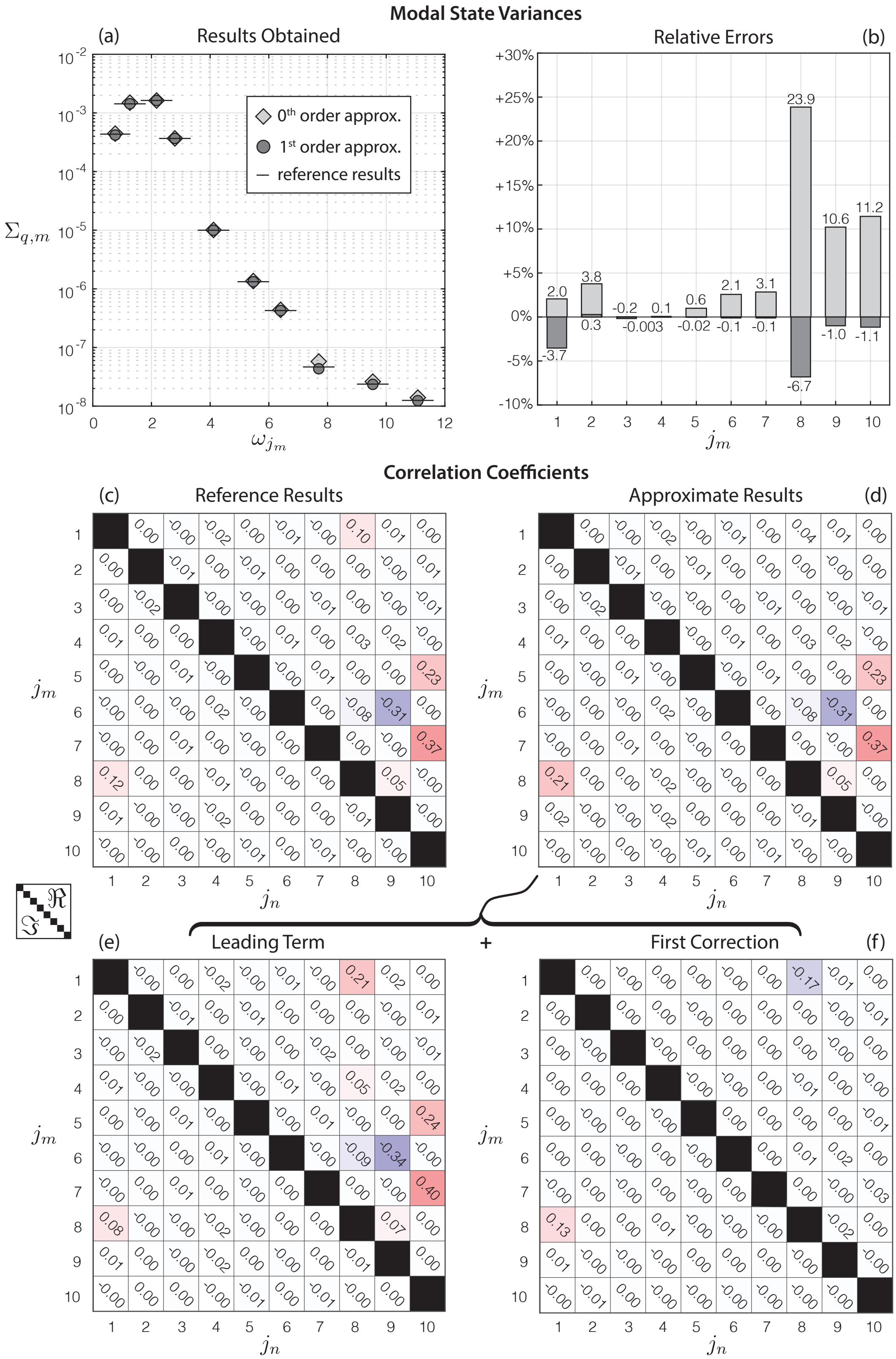

Figure 5: Variances of the modal state responses – (a) reference and approximate results at 0^{th} and 1^{st} order, (b) relative errors of each approximation. Correlation coefficients of the modal state responses – (c) reference results, (d) approximate results at first order, decomposition of (d) into (e) the leading term and (f) the first correction. Top right and bottom left triangular zones in these charts are for the real and the imaginary parts of the coefficients, respectively.

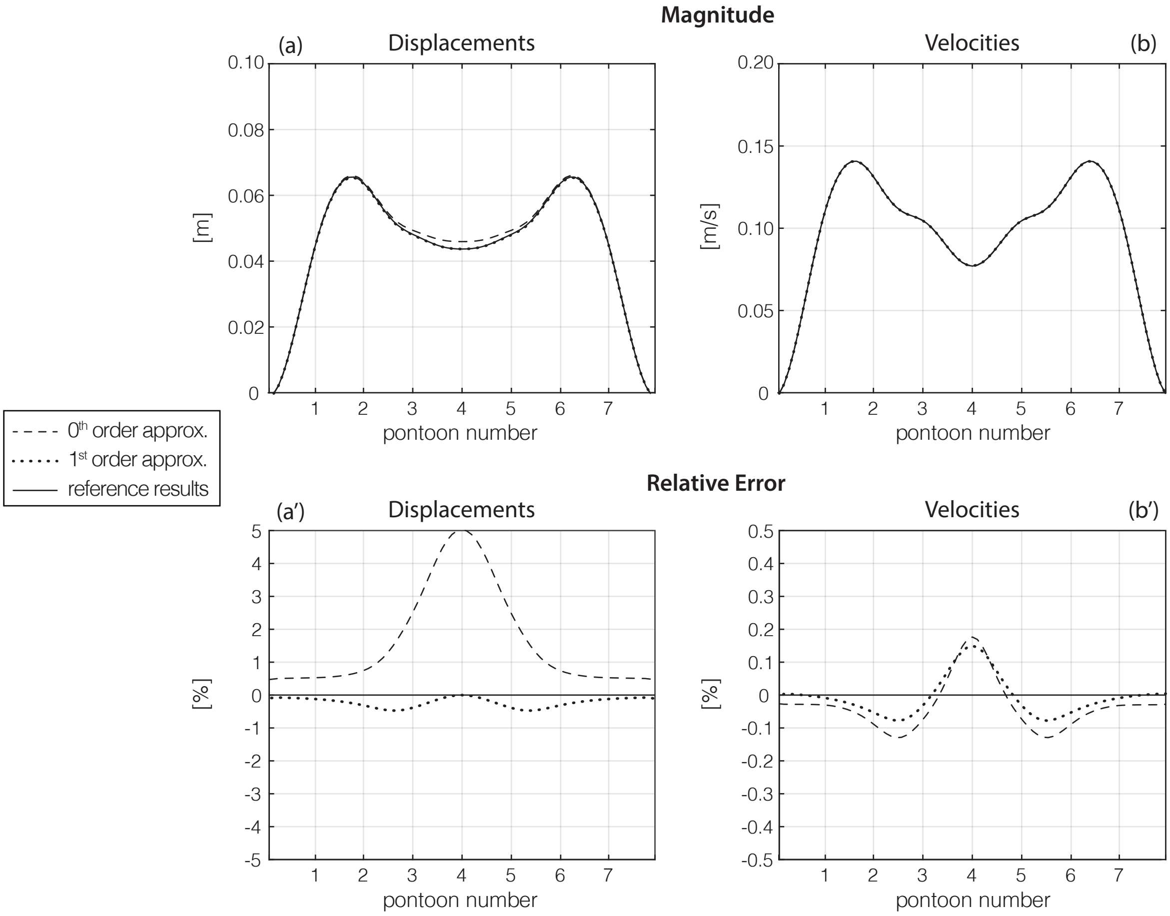

Figure 6: Reference and approximate magnitudes of (a) the displacements and (b) the velocities experienced by the bridge under wave loads, along with the relative errors committed on the magnitudes of (a') the displacements and (b') the velocities by each formulation.